

Design and Implementation of New Planar Massive MIMO Systems for 5G Wireless Networks Extending Omnet++ Simulator

Vincenzo Inzillo
DIMES, University of Calabria
Via P.Bucci, Rende (CS), Italy
Email: v.inzillo@dimes.unical.it

Florian De Rango
DIMES, University of Calabria
Via P.Bucci, Rende (CS), Italy
Email: derango@dimes.unical.it

Alfonso Ariza Quintana
University of Malaga
Av. De Cervantes, Malaga, Spain
Email: aarizaq@uma.es

Luigi Zampogna
University of Calabria
Via P.Bucci, Rende (CS), Italy
Email: luigizampogna@gmail.com

Abstract—The progress accomplished in the modern wireless network are leading to the development of efficient antenna devices that are able to achieve high level requirements with regard to the 5G next generation systems. Although a significant number of theoretical recommendations can already be found in this context, the most known used network simulators do not provide for a support concerning the most recent wireless network requirements like the IEEE802.11ac and, simultaneously, they do not offer the possibility to use the latest massive MIMO (Multiple Input Multiple Output) antenna systems. In view of this, we propose to extend the default features provided by the Omnet++ network simulator with the intention of actualizing the existing simulation instruments to be suitable also for 5G wireless network communication systems.

Index Terms—Massive, MIMO, IEEE802.11ac, Planar, Array

I. INTRODUCTION

Nowadays, the necessity for fulfilling high requirements associated with the management of wireless traffic is continually increasing. In terms of communication process, the most common technology for wireless systems deals with the use of a single antenna both for the transmitter and the receiver. All of these types of systems are usually known as SISO (One Input Single Result). However, presently, significant advancements have been accomplished in this field for the purpose to produce more versatile systems that have the capability to improve the performance of the original technology.

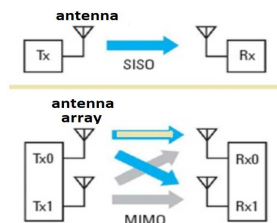


Fig. 1: SISO and MIMO example schema.

In this regard, more sophisticated systems like the MIMO have been introduced. As it can be noted in Fig. 1, MIMO

exploit multiple antennas at the transmitter and the receiver with the aim to considerably enhance the SISO performance [1]. MIMO represent a sort of evolution related to the use of directional antennas and the most recent SAS (Smart Antenna Systems) technology that could bring to accommodate high QoS (Quality of Service) requirements in spite of the omnidirectional systems that usually offer limited functionalities [2], [3] also in high-mobility environments [4]–[6] significantly limiting the network scalability especially in terms of routing [7], [8]. In the Vehicular Ad-Hoc Networks (VANETs), for example, using omnidirectional antennas, connections between vehicles and vehicle and infrastructure devices are unstable because of the high mobility of nodes. Thus, if the contents to be distributed need of a certain level of QoS, heterogeneous metrics have to be considered to follow the dynamics of the network. For these reasons, for building up an efficient routing, it is important to consider different QoS metrics coming from different layers [9], [10]. However, the classical directional approaches are not suitable for satisfying the requirements for the next generation wireless communication systems technology. For this purpose, the massive MIMO technology has been recommended as efficient solution for achieving the 5G requirements especially because of the high antenna gain and high data rate that this kind of systems are able to provide [11]. The term massive, is referred to the large number of antenna elements employed in the hardware; indeed, it is known that, for obtaining high benefits in terms of throughput, a massive amount of radiating element is required; however, in the most recent massive MIMO versions, this number is not less than 70-80 [12]. The use of a large number of antennas stems from the fact that, theoretically, as the amount of elements improves also the total gain of the system grows up. Massive MIMO systems are highly recommended by the latest IEEE802.11ac standard specifications for achieving high throughput requirements in beamforming contexts. The beamforming is defined as the capability of a node to scan and driving the antenna beam pattern toward a certain area or a set of directions. One of the most common problem in this field is represented by the fact that, actually, only

an extremely limited amount of network simulators allow to emulate these very complex technologies. Unfortunately, in such cases, with regard to these network simulators, the cost of the license allowing the end user to access to the 5G package modules, could result very expensive [13]. For this reason, in the present paper, we propose to enhance the features of one of the most used open source network simulator, that is the Omnet++ network simulator [14], by designing three different massive MIMO uniform planar technology modules: the URPA (Uniform Rectangular Linear Array), the UHPA (Uniform Hexagonal Linear Array), and the UCPA (Uniform Circular Linear Array).

II. THE MASSIVE MIMO SYSTEMS

Massive MIMO is a rising technology, that considerably enhances the basic MIMO features. With massive MIMO, are usually indicated the whole of systems that uses antenna arrays with at least few hundred antennas, simultaneously serving multiple terminals in the same time frequency resource.

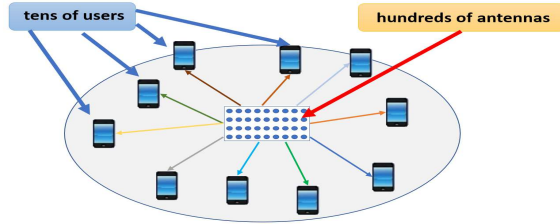


Fig. 2: Massive MIMO operation principle.

The Fig. 2 illustrates the basic operating principle of a massive MIMO; few users are served from a macro-device having a large number of base stations (antennas). Generally, massive MIMO is an instrument that allows to enable the development of future broadband (fixed and mobile) networks which will satisfy special requirements in terms of energy efficiency, security, and robustness. Structurally, a massive MIMO system consists of a group of small (relatively) antennas, supplied from an optical or electric digital bus that operates simultaneously related to a certain task. Massive MIMO, as well as the SAS systems are able to well exploit the SDMA (Spatial Division Multiple Access) allowing for an efficient resource channel utilization, both on the uplink and the downlink [15], [16]. In conventional MIMO systems, like the LTE (Long Term Evolution), the base station transmits waveforms depending on terminals channel response estimation, then, these responses are quantized by some processing units and sent out back to the base station. Fundamentally, this is not possible in massive MIMO systems [17], especially concerning high-mobility environments [18], because optimal downlink pilots should be mutually orthogonal between the antennas. Therefore, in spite of the difficult hardware and designing implementation, these systems are becoming increasingly prevalent in the modern applications due to the great benefits that could introduce; in particular, Massive MIMO can increase the wireless channel capacity up to 10 times and the radiated energy-efficiency up

to 100 times with respect to the traditional LTE systems. This translates into higher gains and higher performance. However, the employment of these systems entails a series of issues that should be properly considered, for example, the interferences between terminals increase as the data rate increases. Other issue is the fact that terminals consume a lot of energy during the communication process in spite of the well SDMA exploitation. Finally, the difficult for designing a system of limited size grows up with the number of antennas. For this reason it is necessary to find a trade-off between the number of elements and the requirements.

III. PLANAR MASSIVE MIMO AND MATHEMATICAL ANALYSIS

From an architectural point of view, a massive MIMO is structured depending on the geometry pattern that is able to form. There exist several design configurations that usually are function of the kind of application to which these systems are destined. Anyway, in this paper, we consider three different types of planar antenna arrays: the URPA, the UHPA and the UCPA. The following subsections synthesize the main feature of the mentioned configurations.

A. Massive MIMO URPA

The Uniform Rectangular Planar Array technology, is the most simple planar massive MIMO configuration. The geometry pattern in this case is consist of a simple matrix within which the antenna elements are placed.

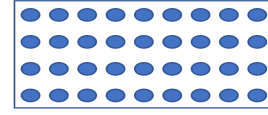


Fig. 3: Massive MIMO URPA example.

The Fig. 3 illustrates an example of massive MIMO URPA configuration. Basically, a URPA is a two-dimensional matrix filled with a certain number of antenna elements (the circles in the figure) both along the x and the y axis; these antenna elements are equally spaced between each one and this spacing is usually expressed in wavelengths. If we denote the number of elements placed on the x axis with M (the rows of the matrix) and with N the number of antennas lying in the y axis (the columns of the matrix), the total number of elements of the URPA is given by:

$$NumElements = M \times N \quad (1)$$

Where M and N are arbitrary integers typically higher than 1. In the first versions of the URPA, M and N were identical and limited to 8; in the modern application M and N are commonly different and chosen between 8 and 12. In general, the radiation field formed by the antenna elements (known also with the term *element factor*) is given by:

$$E_m(r, \theta, \phi) = A \times f(\theta, \phi) \frac{e^{-jkr}}{r} \quad (2)$$

In the eq.2, A is the nominal field amplitude, $f(\theta, \phi)$ is the radiation field pattern, and r is the radial distance between the element and the reference point, that highlights the decrease of the field in function of the distance. According to the pattern multiplication principle, the antenna array total electrical field can be expressed as:

$$E_{TOT} = E_m \times AF(\theta, \phi) \quad (3)$$

The term $AF(\theta, \phi)$ is also known as *array factor* and it depends on the geometry structure of the array. In the case of URPA, the array factor equation is very similar to the Uniform Linear Array (ULA) with the only difference that is designed by considering two dimensions:

$$AF_{URPA}(\theta, \phi) = \left[\frac{\sin\left(\frac{M\psi_M}{2}\right)}{\sin\left(\frac{\psi_M}{2}\right)} \right] \left[\frac{\sin\left(\frac{N\psi_N}{2}\right)}{\sin\left(\frac{\psi_N}{2}\right)} \right] \quad (4)$$

With:

$$\psi_M = kd \sin \theta \cos \phi + \beta_M, \quad \psi_N = kd \sin \theta \sin \phi + \beta_N \quad (5)$$

$$\beta_M = -kd \sin \theta_0 \cos \phi_0, \quad \beta_N = -kd \sin \theta_0 \sin \phi_0 \quad (6)$$

The terms ψ_M and ψ_N indicate the array phase along the x and the y axis respectively while the terms β_M and β_N denote the scanning steering factors along x and y in function of the steering angle θ_0 ; finally, ϕ_0 is the azimuthal elevation steering angle term. Observe that the array factor expression related to eq. 4 is not normalized with respect to M and N . The overall gain of the URPA is expressed by the following:

$$G(\theta, \phi) = \frac{4\pi |f(\theta, \phi) AF(\theta, \phi)|^2}{\int_{\phi=0}^{2\pi} \int_{\theta=0}^{\pi} |f(\theta, \phi) AF(\theta, \phi)|^2 \sin \theta d\theta d\phi} \quad (7)$$

The eq. 7 is the generic expression of the gain valid for all antenna types and is function of the element factor and the array factor. If the antenna elements are isotropic we have $f(\theta, \phi) = 1$ and the gain becomes :

$$G(\theta, \phi) = D(\theta, \phi) = \frac{4\pi |AF(\theta, \phi)|^2}{\int_{\phi=0}^{2\pi} \int_{\theta=0}^{\pi} |AF(\theta, \phi)|^2 \sin \theta d\theta d\phi} \quad (8)$$

The eq. 8 also expresses the directivity of the antenna; thus, from antenna array theory it is possible to obtain the expression which correspond the maximum gain in case of isotropic antenna elements:

$$G_{MAX}(\theta, \phi) = \frac{4\pi \times NumElements^2}{\int_{\phi=0}^{2\pi} \int_{\theta=0}^{\pi} |AF(\theta, \phi)|^2 \sin \theta d\theta d\phi} \quad (9)$$

Indeed, the maximum gain is the value corresponding to the maximum value of the array factor that in the case of the URPA is:

$$AF_{MAX}(URPA) = AF_{MAX}(ULA) = NumElements \quad (10)$$

Note that the maximum value of the array factor for URPA is the same for the ULA and it is equal to the total number of elements of the system. However, from theory, it is known that in the eq. 9 it is not possible to approximate the term $AF(\theta, \phi)$ to $NumElements$ because is function of θ and ϕ which in turn determine the dependency parameters of the double integral.

B. Massive MIMO UHPA

A UHPA configuration, usually, consists of M hexagonal rings, each one having a total number of $6m$ where m is the m -th ring of the system; the antenna elements are uniformly distributed in the hexagonal side.

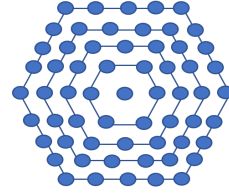


Fig. 4: Massive MIMO UHPA example.

In case of isotropic elements, because the excitation amplitude is set to 1, the array factor can be expressed as the following expression:

$$AF_{UHPA} = \sum_{m=-M}^M e^{j\pi[mv_y - \frac{N}{2}v_x - \frac{m}{2}v_x]} \sum_{n=0}^N e^{j\pi n v_x} \quad (11)$$

Where:

$$N = 2M - |m|; \quad v_x = \sin \theta \cos \phi; \quad v_y = \sin \theta \sin \phi \quad (12)$$

Note that in eq. 11 the dependence on θ and ϕ is omitted and furthermore the steering factor for beam scanning is not considered, while v_x and v_y denote the planar vectorial components along the x and the y axis respectively. The maximum theoretical gain is the same of the URPA case, except from the array factor term.

C. Massive MIMO UCPA

The geometry structure of a Uniform Circular Planar Array is very similar to a UHPA, except from the fact that the hexagonal ring is replaced by a circular ring. As assumed for the UHPA we can consider the widespread configuration having $6m$ antenna elements uniformly placed around the circular edge of the m -th radius.

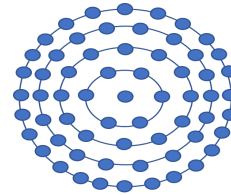


Fig. 5: Massive MIMO UCPA example.

The Fig. 5 illustrates the UCPA configuration that consists of a certain number of circular rings having same center but different radius with the antenna elements placed on the circumference of each ring. Because an UCPA is a particular case of the hexagonal structure, the array factor equation is quite similar to the UHPA expression. In case of isotropic elements the array factor could be expressed by the following:

$$AF_{UCPA} = 1 + \sum_{m=1}^M \sum_{n=1}^{6m} e^{-j(\pi m \sin \theta \cos(\phi - \phi_n) + \beta_M)} \quad (13)$$

Where:

$$\begin{aligned} \beta_M &= \sin \theta_0 \cos(\phi_0 - \phi_n) \\ \phi_n &= \frac{2\pi n}{6m} = \frac{\pi n}{3m} \end{aligned} \quad (14)$$

The eq. 13 (the dependence on θ and ϕ is omitted) considers the possibility to scan the beam through the use of the term β_M which is function of the steering elevation ϕ_0 . The M and θ_0 are already defined in the previous subsection. From theory is also known that the steering vector and the array factor are closely related to the number of antenna elements, the array configuration and the antenna elements excitation (which in this case is unitary in amplitude). It is easy to conclude that the maximum achievable gain is the same of the UHPA and URPA case. However, as verified for the UHPA, the total number of elements is usually an odd number and depends on the number of circular ring in the structure.

IV. PROPOSED MODEL AND MOTIVATIONS

The latest release of the *Omnet++* simulator (the 5.3 version), does not provide neither for a support to asymmetrical communications and neither for the implementation of the latest IEEE802.11 standards. However, as regards the first aspect, we already designed in [19] a *PhasedArray* SAS module that allows to emulate asymmetrical directional communications also enabling simulation beamforming scenarios. Relative to the second aspect, indeed, *Omnet++* offers a complete support for 802.11b/g and the most recent 802.11n standard; in particular, the latest version of *Omnet++* implements various beamforming features of the 802.11n such as the MAC frame aggregation. Nevertheless, these features are not sufficient for emulating the latest massive MIMO technologies that require the complete design of the IEEE802.11ac standard in terms of physical layer features. In fact, the maximum data rate supported in the *radio* module by the current latest version of *Omnet++* is 54 Mbps, along with a 64-QAM (Quadrature Amplitude Modulation), according to the 802.11n specifications. In view of these issue we aim to extend the *Omnet++* features both by providing a full 802.11ac radio environment and a new massive MIMO antenna module suitable for 5G wireless network environments operating according to the IEEE802.11ac standard.

A. IEEE802.11ac implementation

The first step consists in the implementation of the 802.11ac standard in the physical modules of *Omnet++*. Basically, this process involves modifications as regards two micro-layers: the *error model* and the *modulation*. The error model determines the computation of the BER (Bit Error Rate) and PER (Packet Error Rate) curves and furthermore the error probability evaluation in function of the data rate configurations. Obviously, as already stated, the current error models are determined by considering the maximum data rate of 54 Mbps. For this reason, this aspect should be fixed in order to design a support of data rates in the order of the Gbps. The modulation is the feature that offers the possibility to achieve the data rate values specified for VHT (Very High Throughput) and in the current latest version *Omnet++* is limited to 64-QAM; this aspect determines the data rate upper-bound in the simulations. The family of modules related to the error model and modulation are contained in the *physicallayer* package.

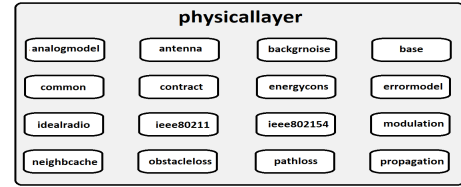


Fig. 6: Physicallayer Omnet++ package structure.

The Fig. 6 illustrates the structure of the *physicallayer* package. The package consists of a remarkable number of subpackages each one determining a feature for the physical layer. Observe that the error model and the modulation micro-layers are contained in this package along with main modelling channel attributes, such as the propagation and the pathloss management. Thus, in order to understand updates introduced for implementing the IEEE802.11ac standard, the following figure shows a block diagram including the main *Omnet++* classes (known also as *modules*) involved in the modification process.

The Fig. 7 represents the module block diagram related to the implementation of the VHT features for the transmitter at physical layer. Each class/module is represented by a rectangle while the dashed-line arrows and the continued-line arrows indicate the *use* and the *inheritance* relationship respectively. The *Ieee80211Radio* module uses the *Ieee80211TransmitterBase* module that is defined by the following NED (Network Description Language) code lines:

Listing 1: Ieee80211TransmitterBase.ned definition

```
module Ieee80211TransmitterBase ... {
parameters:
string opMode @enum("a", "b", "g(erp)", "g(mixed)", "n(mixed)",
-2.4Ghz)", "p", "ac");
string bandName @enum("2.4 GHz", "5 GHz", "5 GHz&20 MHz", "5
GHz&40 MHz", "5 GHz&80 MHz", "5 GHz&160 MHz");
int channelNumber;
modulation = default("BPSK"); }
```

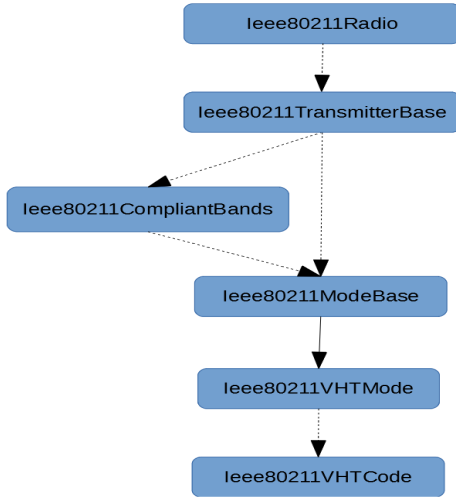



Fig. 7: VHT implementation in the transmitter.

In the Listing 1 the main parameters of the *Ieee80211TransmitterBase* module are illustrated. The *opMode* parameter indicates the kind of IEEE802.11 standard that is determined by a lower-case letter. In this regard, we modified the default code by adding the ac operation mode. Note that also the 5 GHz frequency band configurations have been added. The transmitter uses the class *Ieee80211CompliantBands* for retrieving the available bands and the *Ieee802ModeBase* class obtaining the operation mode. Furthermore, we added all the data rate values provided by the standard by varying the carrier frequency and the number of spatial streams (a small part of these values are illustrated in the Table 1). The *Ieee80211VHTCode* is the module that computes the error probability functions depending on the kind of modulation used in simulation. A similar block diagram could be designed for the receiver.

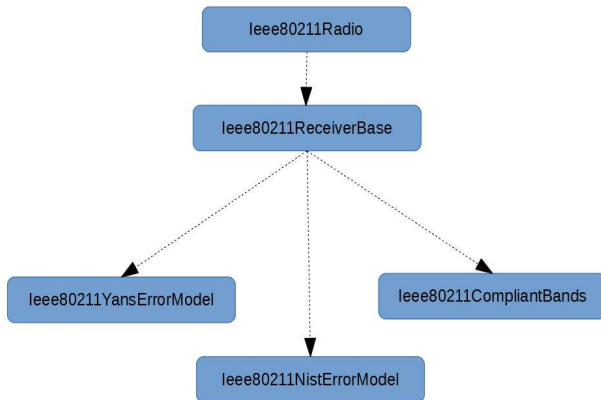


Fig. 8: Error model designing at the receiver.

In the diagram of Fig. 8 it is possible to analyze the hierarchical relationships at the receiver. It is important to highlight

that the error model is mainly used by the receiver rather than the transmitter. *Omnet++* uses some of the error models offered from the *NS3* simulator [20] that are the Yans and the Nist models [21]. Basically, these error modules compute the BER probability values in function of the modulation. For enabling the 802.11ac we extended the default code of *Omnet++* by adding the BER computation functions for 256, 512 and 1024-QAM modulation:

Listing 2: Nist error model BER computation example

```

double Ieee80211NistErrorModel::get256QamBer (double snr)
{
    const {
        double z = std::sqrt (snr / (85.0 * 2.0));
        double ber = 15.0 / 32.0 * 0.5 * erfc (z);
        EV << "256-Qam" << " snr=" << snr << " ber=" << ber;
        return ber; }
}

```

The Listing 2 contains a piece of the full code of the *Ieee80211NistErrorModel* class. The function *get256QamBer* computes and returns the BER relating to a 256-QAM modulation; the BER is evaluated by computing the Zeta function that depends on the SNR (Signal to Noise Ratio).

B. Massive MIMO module design and implementation

Once that we modified the physical layer in order to support the specifications of the VHT standard including the error model and modulations, we designed the massive MIMO antenna modules. The antenna modules are defined in the *physicallayer* package as depicted in Fig. 6. Actually the available antennas in the *physicallayer* package are:

- **ConstantGainAntenna**
- **CosineAntenna**
- **DipoleAntenna**
- **InterpolatingAntenna**
- **IsotropicAntenna**
- **ParabolicAntenna**
- **PhasedArray**
- **MassiveMIMOURPA**
- **MassiveMIMOUHPA**
- **MassiveMIMOUCPA**

The latest four antenna modules enhance the default features of *Omnet++* because they provide for a support for asymmetrical and directional communications scenarios. More specifically, the *PhasedArray* module is the SAS model that we designed in [19]. We provided either for a switched beam version and either for a adaptive array configuration [22]. Anyway, the detailed description of all kinds of antennas is beyond the scope of this paper which instead aims to illustrate the designing feature of the *MassiveMIMOURPA*, *MassiveMIMOUHPA* and *MassiveMIMOUCPA* modules.

Listing 3: MassiveMIMOURPA.ned definition

```

module MassiveMIMOURPA extends AntennaBase {
    parameters:
        double length @unit(m); // length of the antenna
        double distance; // distance between elements
        double freq; // frequency
        double thetazero; // steering angle
        int M; //number of columns
        int N; //number of rows
        .....}
}

```

The listing 3 illustrates the main definition parameters of the *MassiveMIMOURPA* antenna module. Note that the module inherits the basic features of the *AntennaBase* module; besides the main antenna array parameters such as the *length* the *distance* and the *frequency*, the module provides for the setting of the steering angle *thetazero* in order to support the beam piloting; as already mentioned, *M* and *N* represent the number of elements to be placed on the y-axis and x-axis respectively.

Listing 4: MassiveMIMOU CPA.ned definition

```
module MassiveMIMOU CPA extends AntennaBase {
  parameters:
    double length @unit(m); // the length of the single
      antenna
    double distance; // distance between elements
    double freq;
    double thetazero; // the steering angle
    int M; //number of circular rings
    string energySourceModule;
    double interval @unit(s)=default(2s);
    .....}
```

The Listing 2 shows a portion of code extracted by the *MassiveMIMOU CPA* ned definition. The structure of the code is very similar to the URPA definition with the only exception that in this case the main parameter is the number of circular rings *M*; the same strategy has been employed for the definition of the *MassiveMIMOUHPA* module. Therefore, in order to understand the implementation of the logic operations of the modules, the following pseudo-code illustrate a portion of the *MassiveMIMOUHPA.cc* definition:

Algorithm 1 MassiveMIMOUHPA.cc pseudo-code

```
1: procedure INITIALIZE(int stage)
2:   initialize the module
3: end procedure
1: procedure GETMAXGAIN
2:   double maxG;
3:   int numel = getNumAntennas();
4:   double numer = 4 * M_PI * numel * numel;
5:   maxG = 20 * log10(numer/risInt);
6:   return maxG;
7: end procedure
1: procedure COMPUTEGAIN(EulerAngles direction)
2:   const std::complex < double > i(0,1);
3:   double heading = direction.alpha;
4:   for (int m=-emme; m<=emme ; ++m) do
5:     int val = (2*emme) - abs(m);
6:     sum2 = 0;
7:     for (int n=0; n<= val; ++n) do
8:       double aux = (double)n * (sin(heading) *
cos(elevation) + betaM);
9:       complex <double> aux2 = exp(i * M_PI * aux);
10:      sum2 += aux2;
11:    end for
12:  end for
13:  return gain;
14: end procedure
1: procedure COMPUTEINTEGRAL
2:   double risInt = computes the double integral
3:   return risInt;
4: end procedure
```

The algorithm 1 depicts the main functions of the *MassiveMIMOUHPA.cc* class. The function *getMaxGain* computes the maximum gain according the to the eq. 9; the function

getNumAntennas returns the total number of antennas of the massive MIMO; the result of double integral (given by the *risInt* variable) is evaluated by implementing the Simpson method [23] in C++ in the function *computeIntegral*; Observe that the integral could be computed by using some mathematical software tools as MATLAB and then passed to *Omnet++*, but in this case, we decided to implement the evaluation in C++ because the computation is once and because the use of MATLAB with this kind of very complex antenna module could significantly slow down the simulation. Finally, the function *computeGain* evaluates the gain in function of the direction *EulerAngles* components [24] and the steering angle *thetazero* according to the eq. 11; the portion of code of *computeGain* function that is shown in the algorithm 1 is related to the implementation of the summations of the eq. 11.

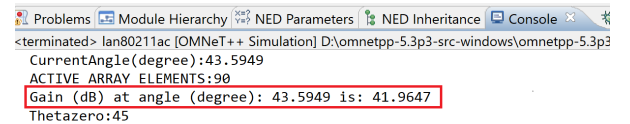
V. MODEL VALIDATION AND SIMULATION RESULTS

The validation of the designed models is accomplished by illustrating some log screens related to the debug runs and by analyzing some useful statistics extracted from the simulations. The following table includes the most important simulation set parameters:

TABLE I: Main simulation parameter set.

Antenna Model	Massive MIMO URPA/UHPA/UCPA
Network Standard	Ieee802.11ac
Num. of elements	90 (URPA), 91 (UHPA), 91 (UCPA)
Steering angle	45°
Carrier freq.	5 GHz
Ch. bandwidths [Mhz]	20, 40, 80, 160
Num. of nodes	20, 50, 100
Data Rates [Mbps]	from 57.8 to 6933.3
Traffic data type	UDP
Sim. Area Size	500 x 500 m
Sim. time	300 s

The simulations have been accomplished by using 20 different seeds and extracting the confidence intervals obtained by the repetitions considering a confidence level set to 95 %. The traffic is represented by UDP (User Datagram Protocol) data packets randomly generated (based on the simulation seed) by different couples of nodes. Therefore, the most of the antenna parameters including the number of elements and the spacing in the system are the same used in [25] with the only exception that we also provided for the beam steering angle setting. For simulations we considered such of the data rates provided by the 802.11ac standard in function of the number of spatial streams. In order to validate the model, the first test consists of the analysis of such run simulation logs:



The screenshot shows a log window with several tabs: Problems, Module Hierarchy, NED Parameters, NED Inheritance, and Console. The Console tab is active, displaying the following text:

<terminated> [an80211ac [OMNeT++ Simulation] D:\omnetpp-5.3p3-src-windows\omnetpp-5.3p3

CurrentAngle(degree):43.5949

ACTIVE ARRAY ELEMENTS:90

Gain (dB) at angle (degree): 43.5949 is: 41.9647

Thetazero:45

Fig. 9: Portion of log extracted by simulations.

Fig. 9 represents a portion of log extracted by a randomly chosen simulation run related to the case of URPA; the result of the log is printed on the console perspective of *Omnet++*; the red rectangle highlights the main line of the log, that displays the result of the computed gain in function of the current angle; the main line synthesizes that the value of the gain corresponding to the angle of 43.5949° is 41.9647 dB; considering the steering angle of 45° we can manually compute the maximum gain that is the gain corresponding to the maximum radiation angle (thus the steering angle) by using the eq. 9 and replancing the terms of the equation with the values used in Tab. 1:

$$G_{MAX}(\theta_0 = 45^\circ, \phi) = \frac{4\pi \times 90^2}{772.97} - \delta_{\theta_0} = \mathbf{42.16 \text{ dB}} \quad (15)$$

Where δ_{θ_0} represents the attenuation in dB related to the steering angle with respect to the maximum gain corresponding to $\theta = 0^\circ$ (which is 42.39 dB). In the eq. 15, the value of 772.97 at the denominator is the result of the double integral computed by the simulator, using the Simpson method. Finally, the gain value of 41.9647 dB related to the angle of 43.5949° is almost about close to the maximum gain value, as we could expect. For a further investigation it is possible to design the same considered massive URPA by using the Sensor Array Analyzer tool provided by MATLAB and compare the values obtained in our case.

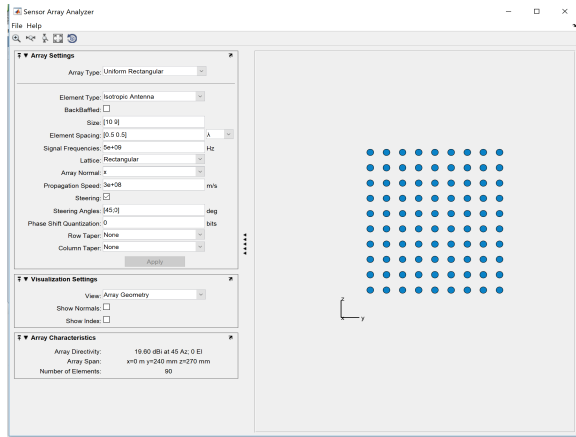


Fig. 10: URPA module using Sensor Array Analyzer.

The Fig. 10 displays the configuration related to our designed antenna model generated by the Sensor Array Analyzer. In the figure, the value of the maximum gain is the value related to the directivity that is 19.60 dBi (power dB value) which corresponds approximately to 42.16 dB. This value is exactly the same value obtained in our simulations. The second phase of the model validation involves the analysis of such simulation statistics extracted from runs. For this purpose we performed the runs by increasing the data rate as well as the channel bandwidth. More specifically, we considered the following configurations: **for 20 MHz:** 57.8 and 115.6 Mbps; **for 40 MHz:** 360 and 720 Mbps; **for 80 MHz:** 1560 and 2340 Mbps; **for 160 MHz:** 5200 and 6933.3 Mbps. Note that the

data rate is increased about twice between each configuration. The used data rate values are extracted from the IEEE802.11ac standard related to the tables having $N_{SS} = 8$ and guard interval of 400 ns. The first analyzed statistic is related to the average SNIR (Signal to Noise Interference Ratio) in function of the data rate and is derived by extracting the *minSNIR* statistic provided by *Omnet++*. The values extracted from the minSNIR histogram are averaged by considering 3 different values of power for the transmitter : 20, 30 and 50 mW. Also consider that we performed the simulations by using a value of background noise set to -110 dBm. This value suggests that the channel is weekly affected from interferences.

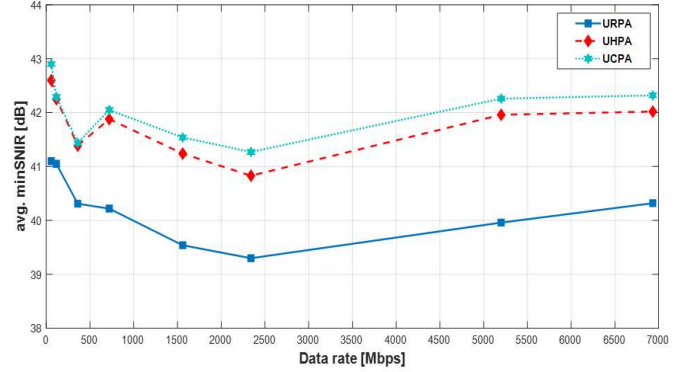


Fig. 11: Average minimum SNIR vs data rate.

The Fig. 11 illustrates the average minimum SNIR in function of the data rate. The curves related to the three different kinds of considered array configurations present a very similar trend. Anyway, for all of the curves, the best case, as we can expect, is registered at the low data rate case; as the data rate enhances the SNIR tends to decrease almost linearly according to the theoretical expectations. However, observe that corresponding to the highest data rates the decreasing trend seems to reverse, especially as regard the URPA curve. This is probably due because of two main reasons: firstly, the bandwidth amplitude related to the highest data rates which is at least double with respect to the other configurations; secondarily, the level of the modulations used for the data rates 5200 and 6933.3 Mbps that are a 64-QAM and a 256-QAM respectively; these modulations can grant similar performance compared to lower data rate configurations that use less level-efficient modulation schemas, especially when the channel is very weekly affected from noise. From Fig. 11 it also can be noted how the UHPA and the UCPA curves for small data rate values are almost overlapping and slightly overhang the URPA curve. In order to validate these results, because we considered the same antenna configurations of the work [25], we can evaluate the maximum gain for each configuration by using the eq. 15 (which considers the steering) also making a comparison with the values obtained in [25]. In particular, the obtained results related to the double integral at the denominator of the eq. 9 for each configuration were: 772.97 for URPA, 768.47 for UHPA and 736.23 for UCPA. By substituting

these values in the eq. 15 we obtained the corresponding maximum gain values: 42.16 dB for URPA, 42.49 dB for UHPA and 42.71 dB for UCPA; these values justify the curves obtained in Fig.11. For a further investigation we extracted the throughput statistics by averaging with respect to the data rate, for each configuration, the throughput vector values provided by *Omnet++* generated by the *thruputmeter* module.

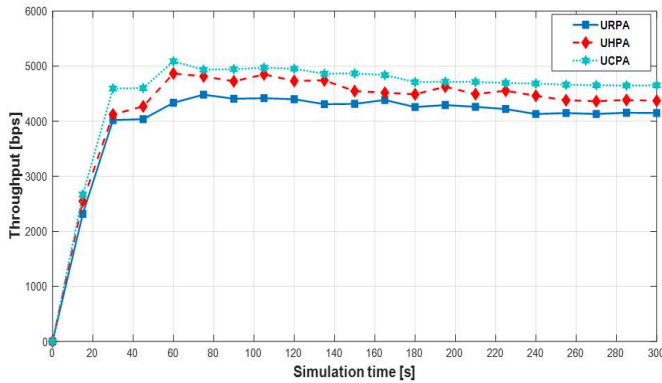


Fig. 12: Planar massive MIMO throughput comparison.

The Fig. 12 compares the throughput curves of the considered configurations in function of the simulation time. Observe how the high similarity between curves related to UHPA and UCPA is maintained compared to Fig. 11 as well as the slight difference in terms of amplitude with respect to the URPA curve.

VI. CONCLUSION

We proposed three different kinds of massive MIMO array with the aim to extend the default features of the *Omnet++* simulator. For testing our designed modules, we modified the default error models provided by *Omnet++* in order to make the simulator compatible with the 802.11ac standard. For validating the proposal, we compared our designed modules with the Sensor Array Analyzer tool and then, we analyzed the statistics generated by *Omnet++* also making some throughput comparisons between the different antenna modules. The main goal of the present paper was to provide for an open source simulation instrument able to emulate the future wireless network scenarios, in order to overcome the main issues in this field, including the expensive license costs of the very few simulation companies that offer these kinds of features; at the same way, this work aims to upgrade the set of features offered by *Omnet++* for the purpose of enhancing the potentialities of the simulator and supporting the compatibility with the most recent 5G network technologies. The full *Omnet++* code of the designed modules may be requested by sending an email to one of the authors of the present paper.

REFERENCES

[1] E. Björnson, L. Sanguinetti, J. Hoydis, and M. Debbah, "Optimal design of energy-efficient multi-user mimo systems: Is massive mimo the answer?" *IEEE Transactions on Wireless Communications*, vol. 14, 2015.

[2] M. Jain and R. Agarwal, "Capacity & coverage enhancement of wireless communication using smart antenna system," in *Advances in Electrical, Electronics, Information, Communication and Bio-Informatics (AEE-ICB)*, 2016 2nd International Conference on. IEEE, 2016, pp. 310–313.

[3] A. Senapati, K. Ghatak, and J. S. Roy, "A comparative study of adaptive beamforming techniques in smart antenna using lms algorithm and its variants," in *Computational Intelligence and Networks (CINE)*, 2015 International Conference on. IEEE, 2015, pp. 58–62.

[4] P. Fazio, F. De Rango, and C. Sottile, "An on demand interference aware routing protocol for vanets," *Journal of Networks*, vol. 7, 2012.

[5] F. De Rango, F. Veltri, P. Fazio, and S. Marano, "Two-level trajectory-based routing protocol for vehicular ad hoc networks in freeway and manhattan environments," *Journal of Networks*, vol. 4, 2009.

[6] P. Fazio, F. De Rango, and C. Sottile, "A new interference aware on demand routing protocol for vehicular networks," in *Performance Evaluation of Computer & Telecommunication Systems (SPECTS)*, 2011 International Symposium on. IEEE, 2011.

[7] F. De Rango, M. Gerla, and S. Marano, "A scalable routing scheme with group motion support in large and dense wireless ad hoc networks," *Computers & Electrical Engineering*, vol. 32, 2006.

[8] B. Zhou, Y.-Z. Lee, M. Gerla, and F. De Rango, "Geo-lanmar: a scalable routing protocol for ad hoc networks with group motion," *Wireless Communications and Mobile Computing*, vol. 6, 2006.

[9] C. Sottile, A. F. Santamaria, and S. Marano, "A reactive routing protocol for vanets based on composite metric concept," in *Performance Evaluation of Computer and Telecommunication Systems (SPECTS 2014)*, International Symposium on. IEEE, 2014.

[10] A. F. Santamaria, C. Sottile, F. De Rango, and S. Marano, "Safety enhancement and carbon dioxide (co₂) reduction in vanets," *Mobile Networks and Applications*, vol. 20, 2015.

[11] A. F. Molisch, V. V. Ratnam, S. Han, Z. Li, S. L. H. Nguyen, L. Li, and K. Haneda, "Hybrid beamforming for massive mimo: A survey," *IEEE Communications Magazine*, vol. 55, 2017.

[12] E. Björnson, E. G. Larsson, and M. Debbah, "Massive mimo for maximal spectral efficiency: How many users and pilots should be allocated?" *IEEE Trans. on Wireless Communications*, vol. 15, 2016.

[13] H. Zhang, N. Liu, Chu *et al.*, "Network slicing based 5g and future mobile networks: mobility, resource management, and challenges," *IEEE Comm. Magazine*, vol. 55, 2017.

[14] Omnet++, "5.3 release," 2018.

[15] H. Yan and D. Cabric, "Digital predistortion for hybrid precoding architecture in millimeter-wave massive mimo systems," in *Acoustics, Speech and Signal Processing (ICASSP)*, 2017 IEEE International Conference on. IEEE, 2017.

[16] G. Yang, C. K. Ho, R. Zhang, and Y. L. Guan, "Throughput optimization for massive mimo systems powered by wireless energy transfer," *IEEE Journal on Selected Areas in Communications*, vol. 33, 2015.

[17] J. A. Zhang, X. Huang, V. Dyadyuk, and Y. J. Guo, "Massive hybrid antenna array for millimeter-wave cellular communications," *IEEE Wireless Communications*, vol. 22, 2015.

[18] V. Jungnickel, K. Manolakis, W. Zirwas, B. Panzner, V. Braun, M. Losow, M. Sternad, R. Apelfrojd, and T. Svensson, "The role of small cells, coordinated multipoint, and massive mimo in 5g," *IEEE Communications Magazine*, vol. 52, 2014.

[19] V. Inzillo, F. De Rango *et al.*, "A new switched beam smart antenna model for supporting asymmetrical communications extending inet omnet++ framework," in *SPECTS*. IEEE, 2017.

[20] G. Carneiro, "Ns-3: Network simulator 3," in *UTM Lab Meeting April*, vol. 20, 2010.

[21] G. Pei and T. R. Henderson, "Validation of ofdm error rate model in ns-3," *Boeing Research Technology*, pp. 1–15, 2010.

[22] V. Inzillo, F. De Rango, and A. A. Quintana, "A new variable error metric adaptive beamforming algorithm for smart antenna systems," in *Wireless Communications and Mobile Computing Conference (IWCMC)*, 2017 13th International. IEEE, 2017.

[23] K. Ohta and H. Ishida, "Comparison among several numerical integration methods for kramers-kronig transformation," *Applied Spectroscopy*, vol. 42, 1988.

[24] A. Janota, V. Šimák, D. Nemec, and J. Hrbček, "Improving the precision and speed of euler angles computation from low-cost rotation sensor data," *Sensors*, vol. 15, 2015.

[25] W. Tan, S. D. Assimonis, M. Matthaiou, Y. Han, X. Li, and S. Jin, "Analysis of different planar antenna arrays for mmwave massive mimo systems," 2017.